Growth and characterization of organic 2,3,4-trihydroxybenzophenone single crystals for nonlinear optical applications

M. L. Lima Rose[1,2], T. Suthan[3,*] , C. Gnanasambandam[1], and T. C. Sabari Girisun[4]

[1] Department of Physics & Research Centre, S.T. Hindu College (Affiliated to Manonmaniam Sundaranar University, Tirunelveli), Nagercoil 629002, India
[2] Department of Physics, Malankara Catholic College, Mariagiri 629153, India
[3] Department of Physics, Lekshmipuram College of Arts and Science, Neyyoor, Tamil Nadu 629802, India
[4] Nanophotonics Laboratory, School of Physics, Bharathidasan University, Tiruchirappalli 620024, India

ABSTRACT

The organic compound 2,3,4-trihydroxybenzophenone single crystal was grown by slow evaporation technique. The single-crystal XRD studies reveal that the grown crystal belongs to monoclinic crystal system with centrosymmetric space group C2/c. The functional groups of the grown crystal were analyzed by FTIR and FT-Raman analyses. The transmittance and optical parameters of the grown crystal were analyzed using UV–Vis analysis. The electrical properties of the grown 2,3,4-trihydroxybenzophenone single crystal were analyzed using dielectric measurements. The open-aperture Z-scan method is used to analyze the nonlinear optical absorption and optical limiting properties.

1 Introduction

Organic single crystals are widely used for various applications due to their high significance in different fields. The organic single crystals can be used for technological and optical applications, especially for optoelectronic switching, electro-optic modulation, laser frequency conversion, telecommunications, optical logic gates, laser radiation protection, etc. [1–4]. Nowadays, considerable effort was taken to grow newer promising organic good quality nonlinear optical single crystals. The organic benzophenone derivatives have good optical and biological activities. Many researchers have grown various benzophenone derivative crystals using different methods, and their structural and optical properties were analyzed [5]. A variety of structures and pharmacological activities were observed in the benzophenone derivatives. In 2,3,4-trihydroxybenzophenone, the two benzene rings are inclined at 44.6 (5)° to each other in the crystal structure and the benzoyl group's carbonyl O atom is nearly in the 2,3,4-trihydroxybenzene ring plane. The three hydroxyl groups H atoms are oriented in the same direction around

Address correspondence to E-mail: suthantr@yahoo.co.in

Springer

the ring and form intramolecular and intermolecular hydrogen bonds [6]. The development of a photocatalyst with reasonable photocatalytic performance under both UV and Visible light has received a lot of attention [7]. In the field of optoelectronics, the benzophenone derivative 2,3,4-trihydroxybenzophenone-4-methylol has been widely used as photoresists in microelectronic circuits [8]. The organic 2,3,4-trihydroxybenzophenone can act as a novel reducing agent for the one-step synthesis of size-optimized gold nanoparticles. In the present study, the organic benzophenone derivative 2,3,4-trihydroxybenzophenone single crystals were successfully grown by slow evaporation growth technique. The grown crystal was characterized by single-crystal XRD, FTIR, FT-Raman, UV–Vis, dielectric, and NLO studies.

2 Experimental

The organic 2,3,4-trihydroxybenzophenone were commercially purchased from the Sigma-Aldrich with 99% purity. Various solvents are used for the solubility analyses and finally, ethanol was identified as a good solvent for growing 2,3,4-trihydroxybenzophenone single crystals. The variation of solubility versus temperature is shown in Fig. 1. The solubility of the material increases with an increase in temperature. For the growth of 2,3,4-trihydroxybenzophenone single crystal, the computed amount of 2,3,4-trihydroxybenzophenone and ethanol was stirred persistently to achieve a homogeneous saturated solution. The solution was filtered using the Whatman filter paper and covered with perforated polythene sheets. It was kept in an undisturbed place for crystallization at room temperature. The good quality 2,3,4-trihydroxybenzophenone single crystals were harvested. The photograph of the grown 2,3,4-trihydroxybenzophenone single crystal is shown in Fig. 2.

3 Results and discussion

3.1 Single-crystal XRD

The grown crystal was analyzed by single-crystal XRD using Bruker APEX II single-crystal X-ray diffractometer with MoK$_\alpha$ (λ = 0.717073 Å) radiation. The results show that the grown 2,3,4-
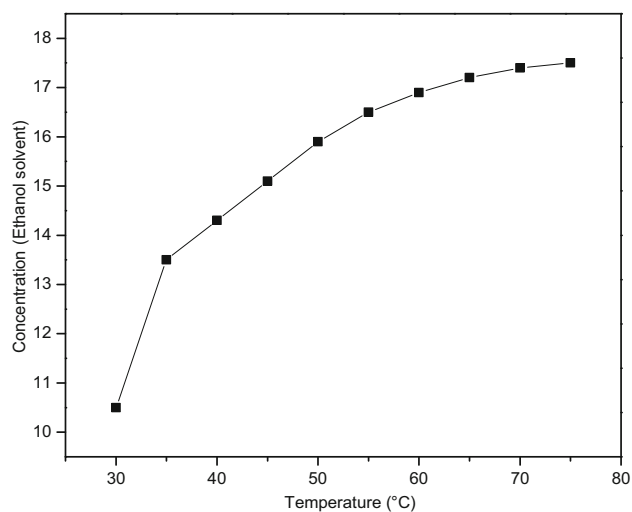

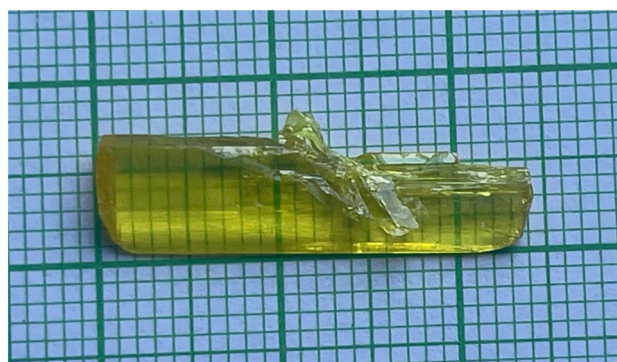**Fig. 1** Solubility graph of 2,3,4-trihydroxybenzophenone single crystal

Fig. 2 Photograph of grown 2,3,4-trihydroxybenzophenone single crystal

trihydroxybenzophenone crystal belongs to the monoclinic crystal system with the centrosymmetric space group C2/c. This is one of the elementary conditions for analyzing the third-order nonlinear properties. The obtained crystallographic parameters of the grown 2,3,4-trihydroxybenzophenone crystal are in good agreement with the previously reported values [6] and it is shown in Table 1.

3.2 FTIR and FT-Raman spectral analyses

The FTIR and FT-Raman spectral analyses were used to identify the functional groups present in the grown 2,3,4-trihydroxybenzophenone single crystal. The FTIR spectrum was obtained by the KBr pellet technique using a Perkin-Elmer FTIR spectrum RXI spectrometer in the region 4000–400 cm^{-1}. The obtained FTIR spectrum of the grown 2,3,4-

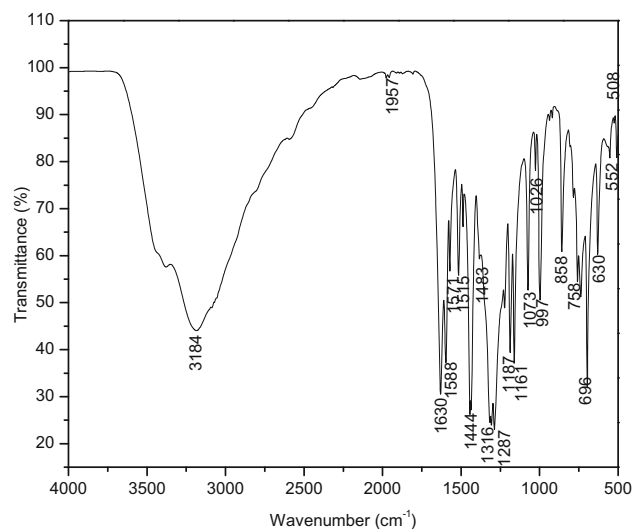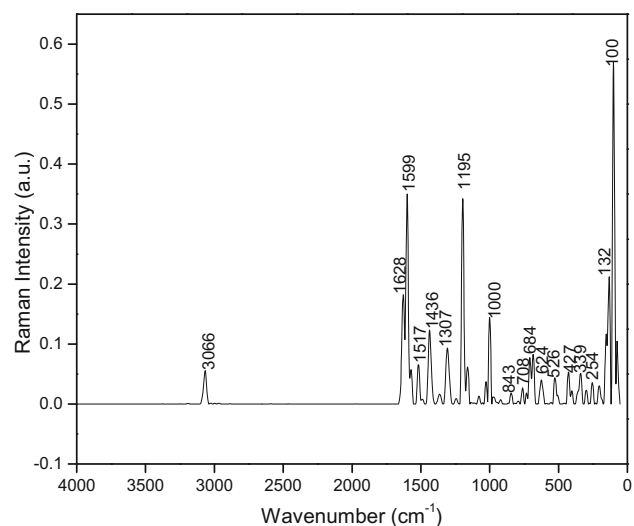**Table 1** Single-crystal XRD data for grown 2,3,4-trihydroxybenzophenone

Unit cell parameters	Reported value	Observed value
a (Å)	33.365	33.52
b (Å)	3.991	4.01
c (Å)	20.837	20.73
α (°)	90	90
β (°)	122.679	122.70
γ (°)	90	90
Volume (Å)^3	2335.5	2346
Crystal system	Monoclinic	Monoclinic
Space group	C2/c	C2/c

Fig. 3 FTIR spectrum of 2,3,4-trihydroxybenzophenone

trihydroxybenzophenone is shown in Fig. 3. The BRUKER RFS FT-Raman spectrophotometer was used for the FT-Raman analysis in the range 4000–500 cm^{-1}. The obtained FT-Raman spectrum of 2,3,4-trihydroxybenzophenone is shown in Fig. 4. The peak observed at 3184 cm^{-1} in FTIR and 3066 cm^{-1} in FT-Raman are due to the presence of OH Stretching vibration. The well-defined peak observed at 1630 cm^{-1} in the FTIR spectrum and 1628 cm^{-1} in the FT-Raman spectrum indicates the presence of amide C=O in the crystal and it is due to the stretching vibration. The sharp peaks identified at 1588 cm^{-1} and 1515 cm^{-1} in FTIR and the peaks at 1599 cm^{-1} and 1517 cm^{-1} in FT-Raman are due to the presence of aromatic C=C bending vibrations. The peaks observed at 1444 cm^{-1} in FTIR and 1436 cm^{-1} in FT-Raman spectra are owing to the presence of O–H in-plane bending vibrations. The presence of phenol O–H in-plane bending vibration is observed at 1316 cm^{-1} in FTIR and 1307 cm^{-1} in the FT-Raman spectrum. The aromatic C–H ring in-plane vibration is observed at 1187 cm^{-1} and 1026 cm^{-1} in FTIR and 1195 cm^{-1} and 1000 cm^{-1} in the FT-Raman spectra. The several peaks observed between 900 and 670 cm^{-1} in both FTIR and FT-Raman spectra are due to the out-of-plane vibration of the C–H ring [9–13]. The obtained FTIR and FT-Raman spectra peaks and their particular assignments are tabulated in Table 2.

3.3 UV–Vis analysis

The organic benzophenone derivative single crystals have good optical properties [14, 15]. The optical transparency and cut-off wavelength of crystals are major components in optical applications. The UV–

Fig. 4 FT-Raman spectrum of 2,3,4-trihydroxybenzophenone

Visible spectrum of a grown crystal was carried out by the Perkin-Elmer model Lambda 35 spectrophotometer. The UV–Visible transmission spectrum of grown 2,3,4-trihydroxybenzophenone crystal is shown in Fig. 5a. The result reveals that the cut-off wavelength was spotted around 405 nm and it has high transmittance. This specifies that the grown 2,3,4-trihydroxybenzophenone single crystal is free from major defects. For optical application, the absorption coefficient (α) of the material is very essential. It can be evaluated from the transmittance (T) and the thickness (t) of the crystal using the formula [16, 17]

Table 2 Molecular vibrational assignments of 2,3,4-trihydroxybenzophenone

Wave number (cm^{-1}) Reference Range	FTIR (cm^{-1})	FT-Raman (cm^{-1})	Functional group	Assignment
3200–2700	3184	3066	O–H	Stretching vibration
1690–1630	1630	1628	Amide C = O	Stretching vibration
1700–1500	1588	1599	Aromatic (C=C)	Bending vibrations
	1515	1517		
1440–1395	1444	1436	Carboxylic Acid O–H	In plane bending Vibrations
1410–1310	1316	1307	Phenol O–H	Bending vibrations
1225–950	1187	1195	Aromatic ring C–H	In plane bending Vibrations
	1026	1000		
900–670	858	843	Aromatic C–H ring	Out of plane bending vibrations
	696	708		
	630	624		

$$\alpha = \frac{2.303 \log\left(\frac{1}{T}\right)}{t}$$

The band gap of the grown crystal was evaluated using the Tauc relation. It is obtained by connecting the absorption coefficient (α) with the photon energy and it is given by

$$\alpha h v = A\left(h v - E_g\right)^m,$$

where hv is the incident photon energy, A is constant, and E_g is the optical band gap of the material. The electronic transition decides the m values, $m = 1/2$ for direct allowed transition, $m = 3/2$ for direct forbidden transition, $m = 3$ for indirect forbidden transition, and $m = 2$ for indirect allowed transition, respectively. The electronic transition of the grown 2,3,4-trihydroxybenzopheone single crystal has a direct allowed transition. Hence $m = 1/2$ is used for the calculation, so the above equation becomes

$$\alpha h v = A\left(h v - E_g\right)^{1/2}.$$

The Tauc graph is drawn between $(\alpha h v)^2$ versus hv and it is shown in Fig. 5b. The optical band gap of the grown 2,3,4-trihydroxybenzophenone single crystal is calculated by extrapolating the linear portion of the graph to the photon energy (hv) [18]. The obtained optical band gap value is 3.06 eV. The extinction coefficient is quite essential for optoelectronic device applications. The measurement of the fraction of light lost during the scattering and absorption per unit thickness of the medium is the extinction coefficient (K). The extinction coefficient is calculated using the relation connecting the absorption coefficient (α) and the wavelength (λ) [19, 20].

$$K = \frac{\lambda \alpha}{4\pi}.$$

Figure 5c shows the plot of extinction coefficient versus wavelength of grown 2,3,4-trihydroxybenzophenone single crystal. Near the optical band edge an exponential part known as the Urbach tail can be found along the absorption coefficient curve. Connecting the absorption coefficient (α) with the photon of energy (hv) near the optical band gap edge gives the Urbach empirical rule [21–24]:

$$\alpha = \alpha_0 \exp\left(\frac{hv}{E_U}\right),$$

where α_0 is the constant and E_U is the Urbach energy. The logarithm on both sides of the above equation gives the equation of a straight line.

$$\ln(\alpha) = \ln(\alpha_0) + \left(\frac{hv}{E_U}\right).$$

The graph between $\ln(\alpha)$ and the incident photon of energy (hv) is shown in Fig. 5d. The reciprocal of the slope gives the Urbach energy. The obtained Urbach energy (E_U) value is 0.18 eV. The result reveals that the grown 2,3,4-trihydroxybenzophenone single crystal has good crystallinity and less disorder near the band edge. Urbach proposed another relation correlating optical band gap E_g and absorption coefficient α is
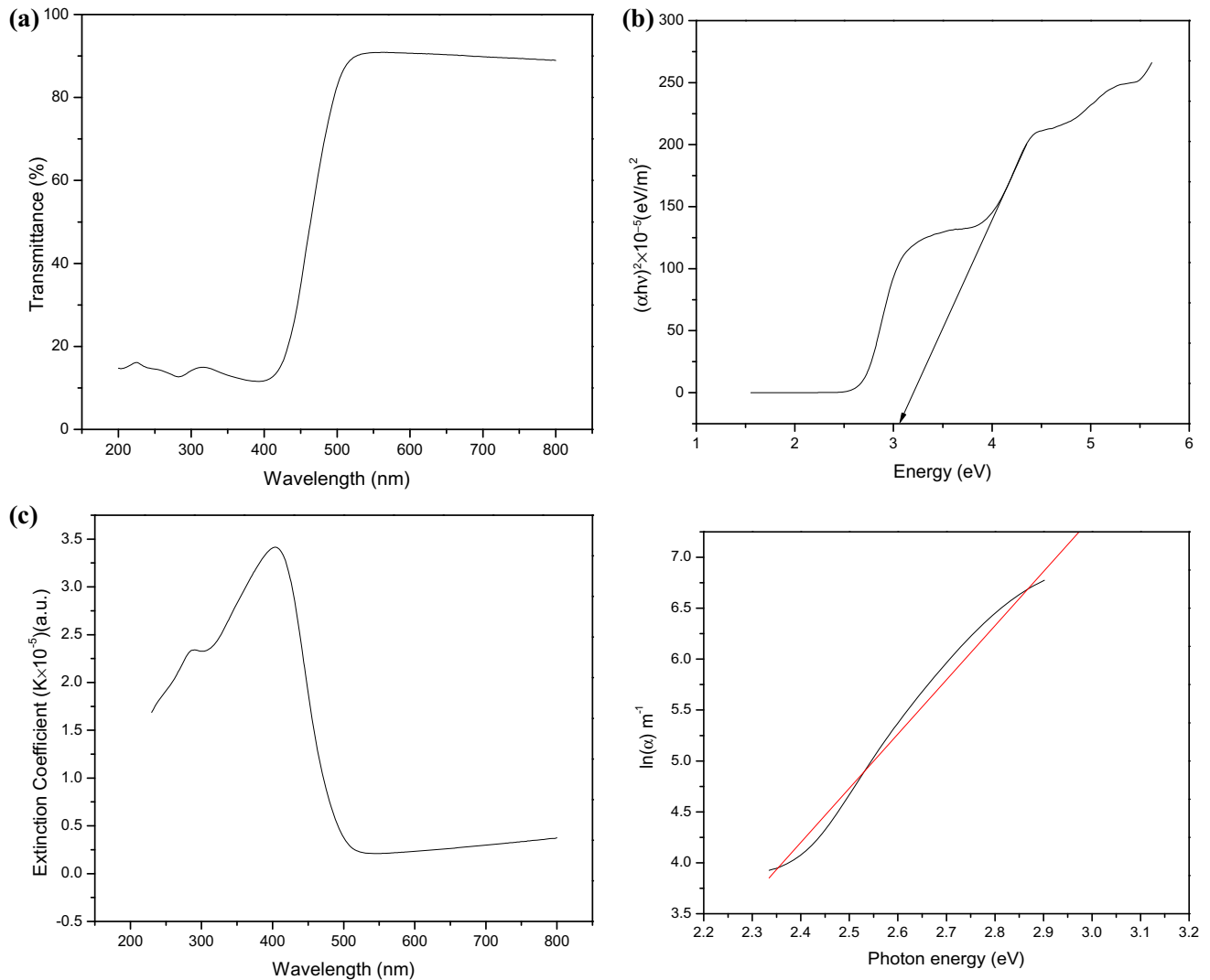
Fig. 5 a UV–Vis transmission spectrum of 2,3,4-trihydroxybenzophenone. **b** Tauc plot between $(\alpha h v)^2$ versus $(h v)$ of 2,3,4-trihydroxybenzophenone. **c** Plot of extinction coefficient versus wavelength of grown 2,3,4-trihydroxybenzophenone single crystal. **d** Plot of $\ln(\alpha)$ versus photon energy of the 2,3,4-trihydroxybenzophenone single crystal

$$\alpha = \beta \exp\left[\frac{\sigma(h v - E_0)}{k_B T}\right],$$

where β is the pre-exponential constant, σ is the steepness parameter, E_0 is the transition energy, and $E_0 = E_g$ for direct allowed transition. Taking the logarithm of the above equation,

$$\ln(\alpha) = \left(\ln(\beta) - \frac{\sigma E_g}{k_B T}\right) + \left(\frac{\sigma(h v)}{k_B T}\right).$$

Comparing $\ln(\alpha)$ of the above two equations,

$$\ln(\alpha_0) = \left(\ln(\beta) - \frac{\sigma E_g}{k_B T}\right)$$

and

$$\left(\frac{h v}{E_U}\right) = \left(\frac{\sigma(h v)}{k_B T}\right),$$

where T is the absolute temperature and k_B is the Boltzmann constant. From the above equation, the steepness parameter (σ) can be evaluated:

$$\sigma = \left(\frac{k_B T}{E_U}\right).$$

The obtained value of σ is 0.125. Using this value, the electron–phonon interaction can be calculated using the following formula:

$$E_{e-p} = \frac{2}{3\sigma}.$$

The calculated electron–phonon interaction is 5.319. The various optical parameters are shown in Table 3.

3.4 Dielectric studies

The electric properties of the grown crystal were analyzed by using dielectric studies [25]. The grown 2,3,4-trihydroxybenzophenone single-crystal dielectric measurements were carried out by the conventional parallel plate capacitor method using an Agilent 4284A LCR meter. The grown crystal was coated with good quality graphite to obtain a good conductive layer and it was used for the analyses. The capacitance and dielectric loss were observed for various temperatures versus the frequencies 1 kHz, 10 kHz, 100 kHz, and 1 MHz. From the measured capacitance values, the dielectric constant ε_r can be calculated using the following formula [26–28]:

$$\varepsilon_r = \left(\frac{A_{air}}{A_{crys}}\right)\left(\frac{C_{crys} - C_{air}\left(1 - \frac{A_{crys}}{A_{air}}\right)}{C_{air}}\right),$$

where C_{crys} is the capacitance of the crystal, C_{air} is the air capacitance as the same dimension, A_{air} and A_{crys} are the area of the electrode and area of the crystal, respectively. The ac electrical conductivity was calculated using the following relation:

$$\sigma_{ac} = \varepsilon_0 \varepsilon_r \omega \tan\delta,$$

where ε_0 is the permittivity of free space, ε_r is the dielectric constant, ω is the angular frequency, and $\tan\delta$ is the dielectric loss factor. The graph drawn between temperature versus dielectric constant, dielectric loss, and ac conductivity at different frequencies is shown in Fig. 6a–c. The figure reveals that the dielectric constant and dielectric loss have higher

Table 3 Linear optical parameters of grown 2,3,4-trihydroxybenzophenone

Description	Calculated value
Optical band gap (E_g)	2.7 eV
Urbach energy (E_U)	0.18 eV
Steepness parameter (σ)	0.125
Electron–phonon interaction (E_{e-p})	5.319

value at low frequency. Due to the absence of space charge polarization near the grain boundary interface, the dielectric constants decrease at higher frequencies [29]. At low frequencies, all polarizabilities ionic, electronic, orientational, and space charge polarizations occur [30, 31]. The low dielectric loss at higher frequencies shows that the grown crystal has the high optical quality and effective applications such as nonlinear optic (NLO), electro-optic modulators (EOM), terahertz (THz) wave generators, field detectors, and microelectronics [32]. High optical quality with lesser defect crystals is required for the fabrication of high-speed integrated photonics applications devices. The Arrhenius relation is used to calculate the activation energy (E_a) of the grown 2,3,4-trihydroxybenzophenone single crystal [33, 34] as follows:

$$\sigma_{ac} = \sigma_0 \exp\left(\frac{-E_a}{kT}\right),$$

where σ_{ac} is the ac electrical conductivity, σ_0 is the pre-exponential factor, E_a is the activation energy, k is the Boltzmann constant, and T is the absolute temperature. The Arrhenius plot in between $\ln(\sigma_{ac})$ versus $1000/T$ is shown in Fig. 6d.

$$E_a = -k \times \text{slope}.$$

The activation energy is calculated from the slope for various frequencies (1 kHz, 10 kHz, 100 kHz, and 1 MHz), the obtained values are 1.4, 0.755, 0.329, and 0.30 eV, respectively. The result shows that the activation energy decreases with an increase in frequency. The hopping conduction is the principal mechanism of this decrease in activation energy [33, 34]. The valence electron plasma energy $\hbar\omega_P$ is calculated using the following formula:

$$\hbar\omega_P = 28.8\left(\frac{Z\rho}{M}\right)^{1/2},$$

where Z is the total number of valence electrons, ρ is the density, and M is the molecular weight of the 2,3,4-trihydroxybenzophenone. From the plasma energy the Penn gap (E_P) is calculated.

$$E_P = \frac{\hbar\omega_P}{(\varepsilon_r - 1)^{1/2}}$$

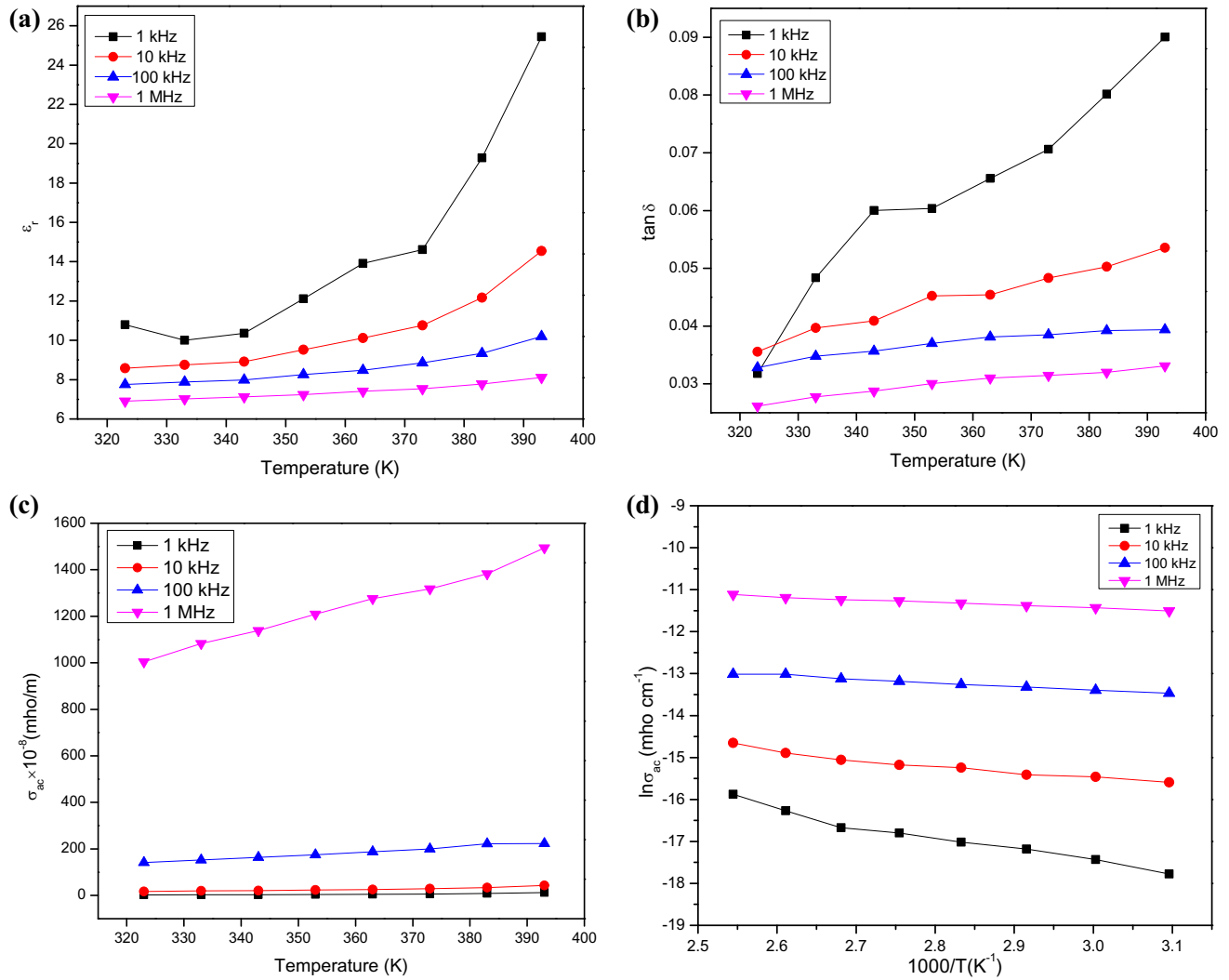The Fermi energy (E_F) is calculated using the following formula:

Fig. 6 a Dielectric constants observed for the 2,3,4-trihydroxybenzophenone single crystal. **b** Dielectric loss observed for the 2,3,4-trihydroxybenzophenone single crystal. **c** The AC electrical conductivities observed for 2,3,4-trihydroxybenzophenone. **d** Arrhenius Plot of $\ln\sigma_{ac}$ versus 1000/T for grown 2,3,4-trihydroxybenzophenone single crystal

$$E_F = 0.2948(\hbar\omega_P)^{4/3}.$$

The grown crystal electronic polarizability is calculated using the following formula:

$$\alpha = \left(\frac{(\hbar\omega_P)^2 S_0}{(\hbar\omega_P)^2 S_0 + 3E_P^2}\right) \times \frac{M}{\rho} \times 0.396 \times 10^{-24} \text{cm}^3,$$

where the constant S_0 is given by,

$$S_0 = 1 - \left(\frac{E_P}{4E_F}\right) + \frac{1}{3}\left(\frac{E_P}{4E_F}\right)^2.$$

Electronic polarizability using the Clausius–Mossotti equation is

$$\alpha = \left(\frac{3M}{4\pi N_a \rho}\right)\left(\frac{\varepsilon_r - 1}{\varepsilon_r + 2}\right)\text{cm}^3,$$

where N_a is the Avogadro number (6.023×10^{23}).

The empirical relation for electronic polarizability is

$$q_0(z,0) = \frac{\beta I_0 L_{\text{eff}}}{\left(1 + \frac{z^2}{z_0^2}\right)}$$

where E_g is the optical band gap (eV). The calculated electronic parameters plasma energy, Penn gap, Fermi energy, and electronic polarizability of the grown 2,3,4-trihydroxybenzophenone crystal are shown in Table 4.

Table 4 Electrical properties of the grown 2,3,4-trihydroxybenzophenone crystal

Parameters	Calculated values
Plasma energy ($\hbar\omega_p$)	14.48 eV
Penn gap (E_P)	5.96 eV
Fermi energy (E_F)	10.41 eV
Electronic polarizability (α)	
Using Valence electron plasma energy	8.75×10^{-23} cm^3
Using Clausius Mosotti equation	9.24×10^{-23} cm^3
Using optical band gap	7.88×10^{-23} cm^3

3.5 Nonlinear optical studies

The Z-scan technique is an active tool to identify the characteristic features of nonlinear interactions and measure third-order nonlinear optical properties such as nonlinear optical absorption (NLOA) and nonlinear refraction (NLR) coefficients of the grown crystal [35]. The third-order NLOA of 2,3,4-trihydroxybenzophenone was measured through the open-aperture Z-scan method. The measurement was carried out using a Q-switched Nd:YAG laser of wavelength 532 nm, an energy of 100 μJ, and a pulse width of 9 ns was used. The grown crystal sample whose linear transmittance is ∼ 65% was used for the analysis. The sample was kept in between the lens and the focal point as the Z-position. The transmitted intensity was measured at different positions by moving the sample along the Z-axis toward or away from the focal point. At each of these positions, the sample experiences different laser intensities. The graph was plotted between the position and normalized transmittance. By fitting the measured Z-scan data to standard NLO transmission equations, we have calculated the NLO coefficients [36–39]. The schematic diagram of the Z-scan setup is shown in Fig. 7.

A setup without an aperture is termed the open-aperture Z-scan technique, where nonlinear absorption of the material can be studied. As no aperture is used in front of the detector, linear transmittance (S) at the detector was assumed to be unity. The various input parameters used in the open-aperture Z-scan technique are shown in Table 5. Saturable absorption (SA) or reverse saturable absorption (RSA) is a nonlinear absorption process in which the transmittance of a material increases or decreases with input fluence, reaching maximum/minimum

transmittance at focus (maximum peak intensity at $z = 0$). The obtained OA Z-scan for the grown 2,3,4-trihydroxybenzophenone crystal appears as a narrow and sharp valley pattern and is shown in Fig. 7a. The minimum transmittance at $z = 0$, i.e., shows higher absorption at focus and it reveals the occurrence of reverse saturable absorption.

The experimental data of normalized transmittance were fitted using the Sheik–Bahae equation as follows:

$$T = \left(\frac{1}{\sqrt{\pi}q_0(z,0)}\right) \int\limits_{-\infty}^{\infty} \ln\left[1 + q_0(z,0)e^{-\tau^2}\right] d\tau,$$

where T is the normalized transmittance of the sample,

$$q_0(z,0) = \frac{\beta I_0 L_{\text{eff}}}{\left(1 + \frac{z^2}{z_0^2}\right)}$$

where β is the effective nonlinear absorption coefficient, Io is the intensity of the laser beam at the focal point, and the sample length,

$$L_{\text{eff}} = \frac{\left\lfloor 1 - e^{(-\alpha l)}\right\rfloor}{\alpha}.$$

The Rayleigh range

$$Z_0 = \frac{\pi\omega_0^2}{\lambda}$$

and ω_0 is the beam waist radius at focus. Here, the experimental data were found to be fitting for the two-photon equation, and thus the grown 2,3,4-trihydroxybenzophenone exhibits a two-photon absorption process. When the laser energy is greater than half of the band gap of the material ($hv > E_g/2$), the two-photon absorption takes place. Here, the material that satisfies this pre-requisite, under green laser (523 nm, 2.33 eV) excitation, an electron absorbs two photons to its band edge involving nonradiative transitions. The estimated effective nonlinear absorption coefficient is termed as β owing to the combined effect of simultaneous or sequential absorption (involving excited state of absorption) of two photons.

The optical limiting measurement can be used to determine the critical power of the laser beam at which nonlinearity begins to impact transmission [40, 41]. The optical limiting curve of a grown crystal drawn between normalized transmittance and input fluence (W/m^2) is shown in Fig. 7b. The figure shows
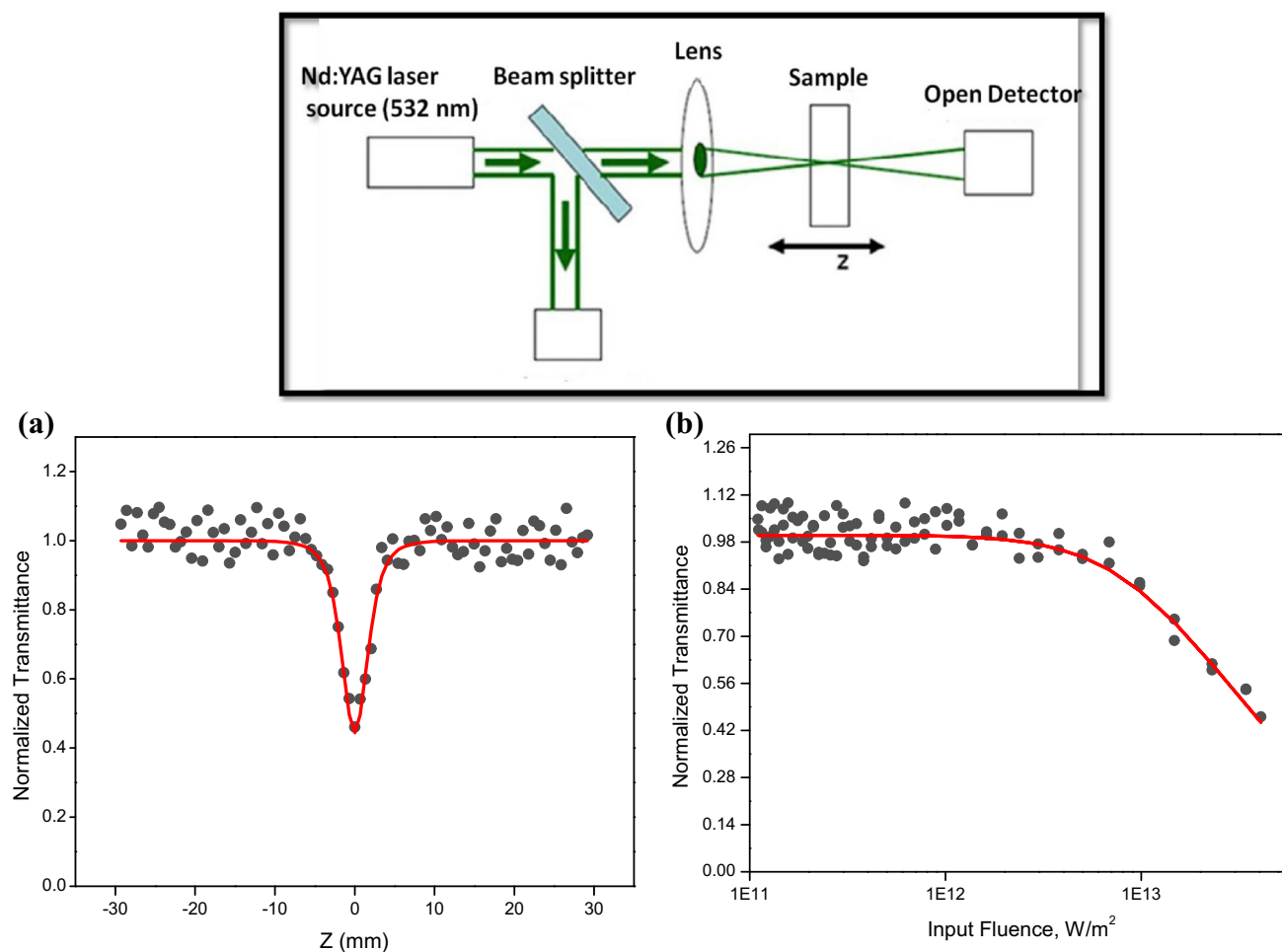
(a)

(b)

Fig. 7 The schematic diagram of Z-scan technique. **a** Open-aperture Z-scan pattern of 2,3,4-trihydroxybenzophenone. **b** Optical limiting cure of 2,3,4-trihydroxybenzophenone

Table 5 Input parameters of the open-aperture Z-scan technique

Laser parameters	Numerical values
Wavelength	532 nm
Frequency	10 Hz
Pulse rate	9 ns
Beam waist	16.9 μm
Path length	1 mm
Rayleigh range	1.69 mm
Focal length	15 cm
Linear transmittance	∼ 65%
Pulse energy	150 μJ
Input intensity	3.69×10^{12} W/m^2

that at low input intensity the material behaves linear, and when the intensity attained is very high the optical transmission of the grown crystal deviates from its linearity and behaves nonlinear. Thus, the grown crystal acts as an optical limiter because it can block the high intensity and transmit the low intensity. The estimated onset optical limiting threshold is 2.45×10^{13} W/m^2. The estimated NLO coefficients are shown in Table 6. The grown 2,3,4-trihydroxybenzophenone exhibits two-photon absorption-induced optical limiting action, it can be used for the development of laser safety devices in laser photonics applications.

4 Conclusion

The organic 2,3,4-trihydroxybenzophenone single crystal was grown by slow evaporation growth technique using ethanol as solvent. The grown crystal was confirmed by using single-crystal XRD analysis. The functional groups were confirmed using FTIR

Table 6 Estimated NLO coefficients of 2,3,4-trihydroxybenzophenone

NLO coefficients	Values
Saturation intensity, I_s	60×10^{11} W/m^2
Nonlinear absorption coefficient, β	0.98×10^{-10} m/W
Onset optical limiting threshold	2.45×10^{12} W/m^2

and FT-Raman analyses. The optical behavior of the grown crystal was analyzed using UV–Vis studies. The optical band gap (E_g), extinction coefficient (K), Urbach energy (E_U), Steepness Parameter (σ), and electron–Phonon interaction ($E_{e\text{-}p}$) were calculated. The dielectric studies reveal that the grown crystal has normal dielectric behavior. The Penn gap (E_p), Fermi energy (E_F), plasma energy, and electronic polarizability (α) were calculated. The open-aperture Z-scan studies reveal that the grown 2,3,4-trihydroxybenzophenone exhibits reverse saturable absorption owing to two-photon absorption. The optical limiting threshold results shows that the grown crystal have potential applications in laser protection devices.

Author contributions

All authors contributed to the study's conception and design. Material preparation, data collection, and analysis were performed by all authors. All authors read and approved the final manuscript.

Data availability

All data generated or analyzed during this study are included in this manuscript.

Declarations

Competing interests The authors declare that they have no conflict of interest.

References

1. T. Suthan, N.P. Rajesh, C.K. Mahadevan, D. Sajan, G. Bhagavannarayana, Mater. Chem. Phys. **30**, 915–920 (2011)
2. D. Prem Anand, M. Gulam Mohamed, S.A. Rajasekar, S. Selvakumar, A. Joseph Arul Pragasam, P. Sagayaraj, Mater. Chem. Phys. **97**, 501–505 (2006)
3. T. Suthan, N.P. Rajesh, J. Cryst. Growth **312**, 3156–3160 (2010)
4. S. Siva Bala Solanki, N.P. Rajesh, T. Suthan, Opt. Laser Technol. **103**, 163–169 (2018)
5. V. Natarajan, M. Arivanandhan, P. Anandan, K. Sankaranarayanan, G. Ravi, Y. Inatomi, Y. Hayakawa, Mater. Chem. Phys. **144**, 402–408 (2014)
6. N. Okabe, H. Kyoyama, Acta Cryst. **E58**, 0565–0567 (2002)
7. S.R. Yousefi, A. Sobhani, H.A. Alshamsi, M. Salavati-Niasari, RSC Adv. **11**, 11500–11512 (2021)
8. Usharani, V. Natarajan, J. Judes, M. Arivanandhan, P. Anandan, S. Natarajan, Optik **127**, 5887–5893 (2016)
9. J. Coates, *Interpretation of Infrared Spectra—A Practical Approach* (Wiley, Chichester, 2000)
10. G. Socrates, *Infrared and Raman Characteristic Group Frequencies: Tables and Charts* (Wiley, Chichester, 2001)
11. V. Krishnakumar, S. Muthunatesan, G. Keresztury, T. Sundius, Spectrochim. Acta A **62**, 1081–1088 (2005)
12. E. Smith, G.G. Dent, *Modern Raman Spectroscopy—A Practical Approach* (Wiley, Hoboken, 2019)
13. S.R. Yousefi, M. Ghanbari, O. Amiri, Z. Marzhoseyni, P. Mehdizadeh, M. Hajizadeh-Oghaz, M. Salavati-Niasari, J. Am. Ceram. Soc. **104**, 2952–2965 (2021)
14. T. Suthan, N.P. Rajesh, C.K. Mahadevan, G. Bhagavannarayana, Spectrochim. Acta Part A **78**, 771–776 (2011)
15. T. Suthan, N.P. Rajesh, C.K. Mahadevan, K. Senthil Kumar, G. Bhagavannarayana, Spectrochim. Acta Part A **79**, 1443–1448 (2011)
16. R.P. Jebin, T. Suthan, T.R. Anitha, N.P. Rajesh, G. Vinitha, J. Mater. Sci. **32**, 3232–3246 (2021)
17. P.P. Abirami Priya, T. Suthan, S. Abraham Thambi Raja, V. Bena Jothy, J. Mater. Sci. **33**, 14214–14227 (2022)

18. S.R. Yousefi, H.A. Alshamsi, O. Amiri, M. Salavati-Niasari, J. Mol. Liquids **337**, 116405 (2021)

19. F.A. Najar, G.B. Vakil, B. Want, Mater. Sci. Pol. **35**(1), 18–31 (2017)

20. Durgadevi, A. Steephen, T. Arumanayagam, J. Mater. Sci. **31**, 18683–18691 (2020)

21. S. Prince, T. Suthan, C. Gnanasambandam, J. Electron. Mater. **51**, 1639–1652 (2022)

22. E.F. Schubert, J.K. Kim, J.-Q. Xi, Phys. Stat. Sol. (B) **244**, 3002–3008 (2007)

23. G. Rajasekar, M.K. Dhatchaiyini, P. Rekha, S. Sudhahar, G. Vinitha, A. Bhaskaran, J. Mater. Sci. **31**, 18732–18744 (2020)

24. M. Anis, S.S. Hussaini, A. Hakeem, M.D. Shirsat, G.G. Muley, Optik-Int. J. Light Electron. Opt. **127**, 2137–2142 (2016)

25. M. Shanmuga Sundaram, V. Vijayalakshmi, P. Dhanasekaran, O.N. Balasundaram, S. Palaniswamy, J. Cryst. Growth **506**(15), 122–126 (2019)

26. T. Suthan, N.P. Rajesh, P.V. Dhanaraj, C.K. Mahadevan, Spectrochimica Acta Part A **75**, 69–73 (2010)

27. T. Suthan, P.V. Dhanaraj, N.P. Rajesh, C.K. Mahadevan, G. Bhagavannarayana, Cryst. Eng. Comm **13**, 4018–4024 (2011)

28. T. Suthan, P.V. Dhanaraj, N.P. Rajesh, Spectrochimica Acta Part A **87**, 194–198 (2012)

29. S. Kalyanaraman, P.M. Shajin Shinu, S. Vijayalakshmi, J. Phys. Chem. Solids **86**, 108–113 (2015)

30. K.V. Rao, A. Smakula, J. Appl. Phys. **36**, 2031–2038 (1965)

31. T. Suthan, N.P. Rajesh, C.K. Mahadevan, G. Bhagavannarayana, Mater. Chem. Phys. **129**, 433–438 (2011)

32. V. Vijayalakshmi, P. Dhanasekaran, Optik **173**, 65–70 (2018)

33. S. Prince, T. Suthan, C. Gnanasambandam, N.P. Rajesh, G. Vinitha, J. Mater. Sci. **33**, 5909–5923 (2022)

34. S. Prince, T. Suthan, S. Goma, C. Gnanasambandam, N.P. Rajesh, J. Mater. Sci. **34**, 165 (2023)

35. T. Arumanayagam, P. Murugakoothan, JMMCE **10**, 1225–1231 (2011)

36. S. Sagadevan, P. Murugasen, Int. J. Mater. Eng. **3**, 159–166 (2015)

37. C. Babeela, N.K. Siji Narendran, M. Pannipara, A.G. Al-Sehemi, T.C. Sabari Girisun, Mater. Chem. Phys. **237**, 121827 (2019)

38. M. Thangaraj, G. Vinitha, T.C. Sabari Girisun, P. Anandan, G. Ravi, Opt. Laser Technol. **134**, 73130 (2015)

39. M. Saravanan, T.C. Sabari Girisun, Mater. Chem. Phys. **160**, 413–419 (2015)

40. A. Pramothkumar, N. Senthilkumar, R. Mary Jenila, M. Durairaj, T.C. Sabari Girisun, I. Vetha Potheher, J. Alloys Compd. **878**, 160332 (2021)

41. M. Monisha, N. Priyadarshani, M. Durairaj, T.C. Sabari Girisun, Opt. Mater. **101**, 109775 (2020)